

Supporting Information (30 pages)

Guest-Dependent Dynamics in a 3D Covalent Organic Framework

Yichong Chen,^{†,‡} Zhao-Lin Shi,^{†,‡,§,£} Lei Wei,^{†,‡} Beibei Zhou,[†] Jing Tan,[†]

Hao-Long Zhou,^{*,†} and Yue-Biao Zhang^{*,†,§,£}

[†]*School of Physical Science and Technology, ShanghaiTech University, Shanghai 201210, China.*

[§]*Joint Laboratory of Low-Carbon Energy Science, Shanghai Advanced Research Institute, Chinese Academy of Sciences, Shanghai 201203, China.*

[£]*University of Chinese Academy of Sciences, Beijing 100049, China*

^{*}*E-mail: zhouhl@shanghaitech.edu.cn or zhangyb@shanghaitech.edu.cn*

[‡]*These author contributed equally.*

Table of Contents

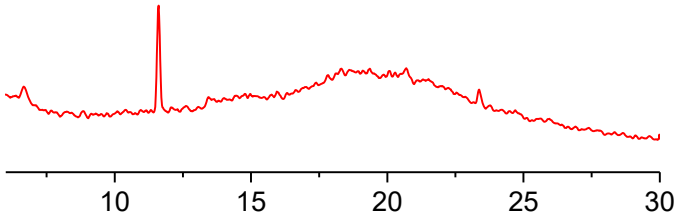
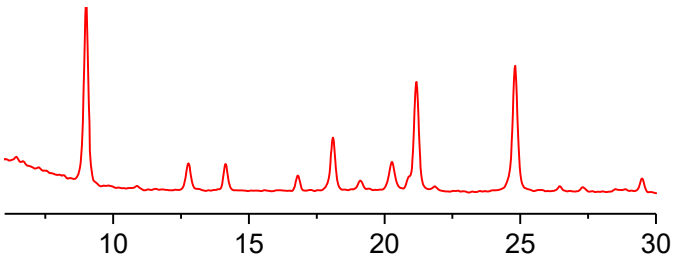
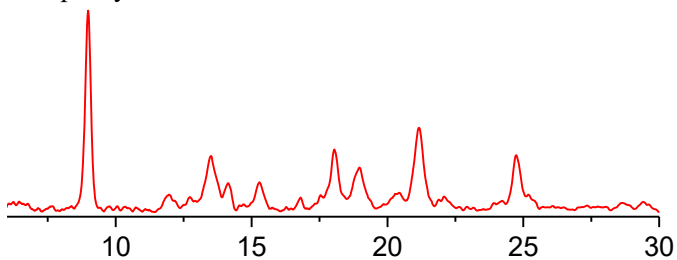
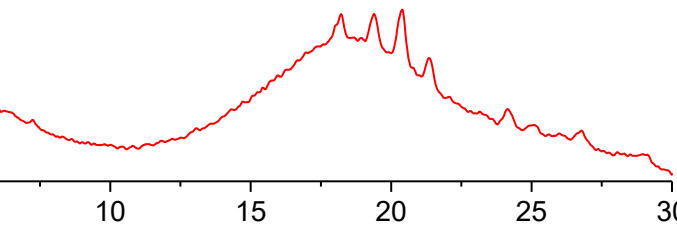
Section S1. Syntheses and Characterization.....	3
Section S2. Structure Modeling and Rietveld Refinements	13
Section S3. Low Pressure Gas/Vapor Adsorption.....	23
Section S4. Gas Adsorption In-Situ PXRD Analyses	28
References	30

Section S1. Syntheses and Characterization

1.1. Materials and Syntheses

Synthesis of COF-300-T. A mixture of TPA (12 mg, 0.089 mmol) and TAM (20 mg, 0.052 mmol) was dissolved in 1 mL of anhydrous 1,4-dioxane within a 2 mL ampulla bottle under sonication. Then 0.2 mL of aqueous acetic acid (3 mol/L) was added into the ampulla bottle, which was then connected to Schlenk line through a rubber hose with stopcock. Cool the ampulla bottle to 77 K by liquid N₂ under high vacuum. Then the ampulla was insulated by turn off the stopcock and allowed return to room temperature. Repeat this process at least three times before the bottleneck of ampulla bottle was quickly sealed with a torch. The reaction was heated at 120 °C for 72 hours, the yellow lump was isolated by hot filtration quickly, and washed with 1,4-dioxane and THF several times to get COF-300-T. (10mg, 38.9% yield based on TPA).

Table S1. Synthesis conditions attempted for COF-300-V.

No.	Reactants			Result
	1,4-dioxane	Cyclohexane	3M AcOH	
1	2mL	0	0.2mL	precipitated after one day, and the resulting product was amorphous
2	1.8mL	0.2mL		precipitated immediately, and the resulting product was not COF-300
				 <p style="text-align: center;">$2\theta/^{\circ}$ (Cu Kα)</p>
3	1.6mL	0.4mL		precipitated immediately, and the resulting product was COF-300
				 <p style="text-align: center;">$2\theta/^{\circ}$ (Cu Kα)</p>
4	1.4mL	0.6mL		precipitated immediately, and the resulting product was COF-300 with impurity
				 <p style="text-align: center;">$2\theta/^{\circ}$ (Cu Kα)</p>
5	1.2mL	0.8mL		precipitated immediately, and the resulting product was not COF-300
				 <p style="text-align: center;">$2\theta/^{\circ}$ (Cu Kα)</p>

Solvent ratio change in the ventilation vial synthesis. To monitor the solvent ratio change, a blank experiments was carried out with the same protocol. The solvent ratio was examined by the ^1H NMR spectroscopy recorded on a Bruker AVANCE III HD 500MHz spectrometer: 30 μL the reactant solvents was mixed with 570 μL of CDCl_3 for measurement. As shown in Fig. S2 and Table S3, the ratio of 1,4-dioxane was reduced after the reaction, indicating a gradually decrease of solubility of the reactants for crashing out the product for higher yield.

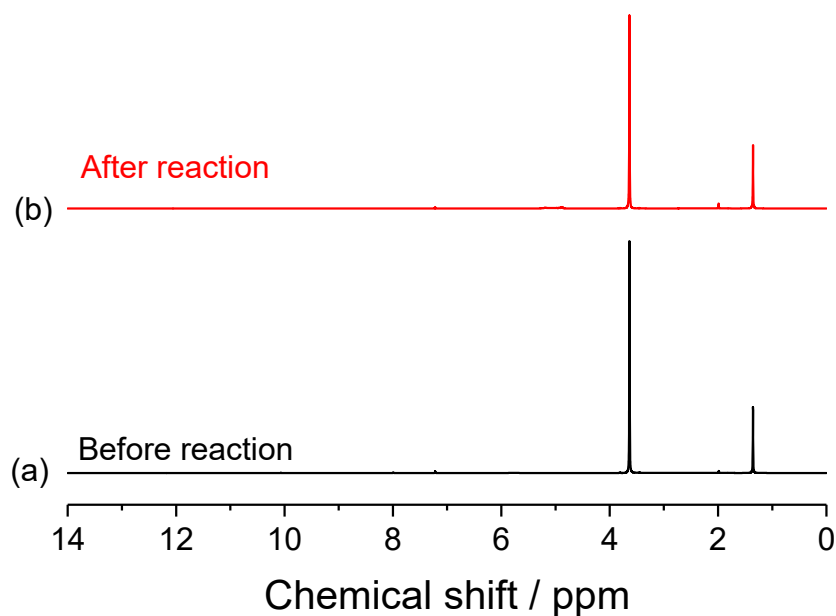


Figure S1. The ^1H NMR spectra of the solvent system optimized for the synthesis of COF-300-V.

Table S2. Chemical shift, assignment and integration of the NMR signals.

chemical shift/ppm	solvent	peak ratio before reaction	peak ratio after reaction
1.43	Cyclohexane	12	12
1.51	Water	0.14	0.13
1.99	Acetic acid	0.35	0.83
3.64	1,4-dioxane	40.49	30.19

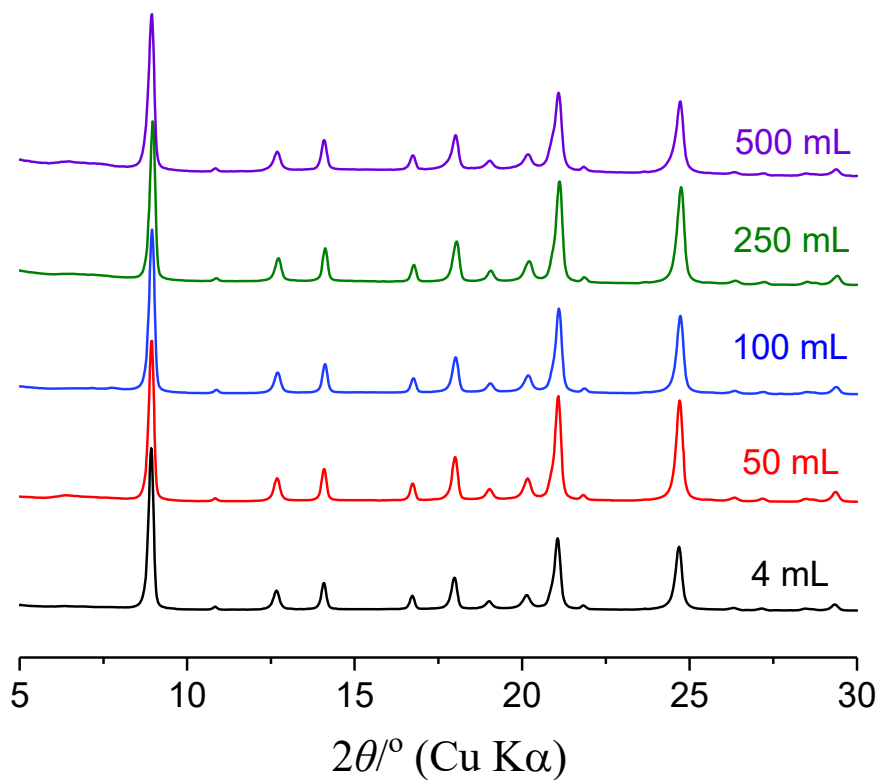


Figure S2. The PXRD pattern of the solvent system optimized for the synthesis of COF-300-V.

Table S3. Scale-up syntheses of COF-300-V

size	Reactants					product weight	yield / %	Space-time-yields(kg/m ³ /d)
	TAM	TPA	1,4-dioxane	cyclohexane	3M AcOH			
500 mL	2.07 g	1.24 g	192 mL	48 mL	48 mL	2.0495 g	76.70	1.366
250 mL	865 mg	519 mg	80 mL	20 mL	20 mL	918.2 mg	83.10	1.224
100 mL	346 mg	208 mg	32 mL	8 mL	8 mL	401.3 mg	91.90	1.337
50 mL	173 mg	104 mg	16 mL	4 mL	4 mL	185.9 mg	85.10	1.239
4 mL	20 mg	12 mg	1.6 mL	0.4 mL	0.4 mL	15 mg	58.40	1.25

1.2 Fourier-Transform Infrared Spectroscopy

The Fourier-transform infrared (FT-IR) spectra were recorded on neat samples in the range of 500–4,000 cm^{-1} on a PerkinElmer FT-IR Spectrometer equipped with single reflection diamond ATR module.

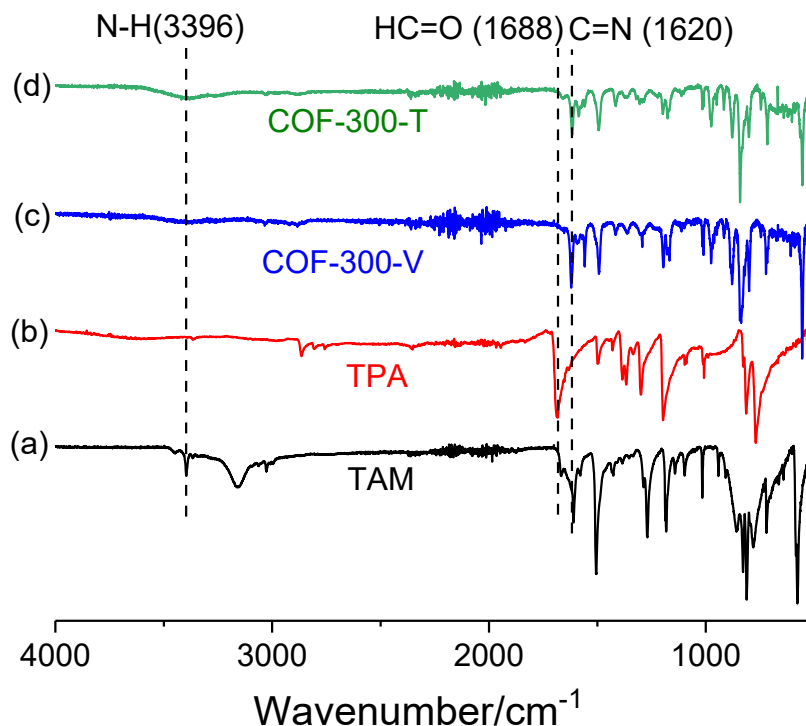


Figure S3. The FT-IR spectrum of the starting materials, TAM (a) and TPA (b), and the products, COF-300-V (c) and the COF-300-T (d). The -C=N- stretching vibration at 1620 cm^{-1} indicated the formation of imine linkages. The bands at 1688 and 3396 cm^{-1} characteristic for aldehyde and amino groups, respectively are marked in dash line. The elimination of these bands in the COF-300-V shows the full conversion of the starting materials and contains less resident terminal group than the COF-300-T.

1.3. Scanning Electron Microscopy

The scanning electron microscopy (SEM) images of COF samples were collected on the on JSM-7800F PRIME extreme-resolution field emission SEM. The sample was suspended in THF and dropped cast on the silicon sample hold for examination under high vacuum. The walking distance and voltage was optimized for the visualization of the crystals.

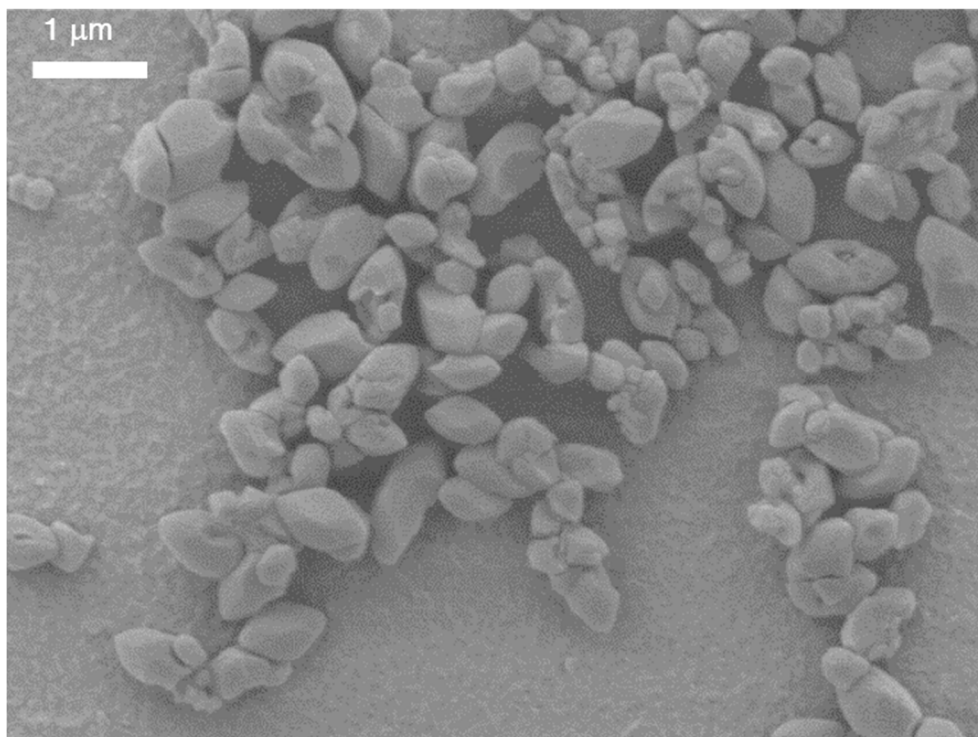


Figure S4. The SEM image of COF-300-V with the scale bar of 1 micrometer. Only a homogenous morphology was observed after exhaustive examination of a range of particles deposited on the sample holder. Well-defined prismatic shapes and the micrometer sizes of $0.5 \times 0.5 \times 1.0 \mu\text{m}^3$ approximately were generally observed in aggregation. Both of the homogenous morphology and well-defined shapes of COF-300-V suggests the high crystallinity and phase purity.

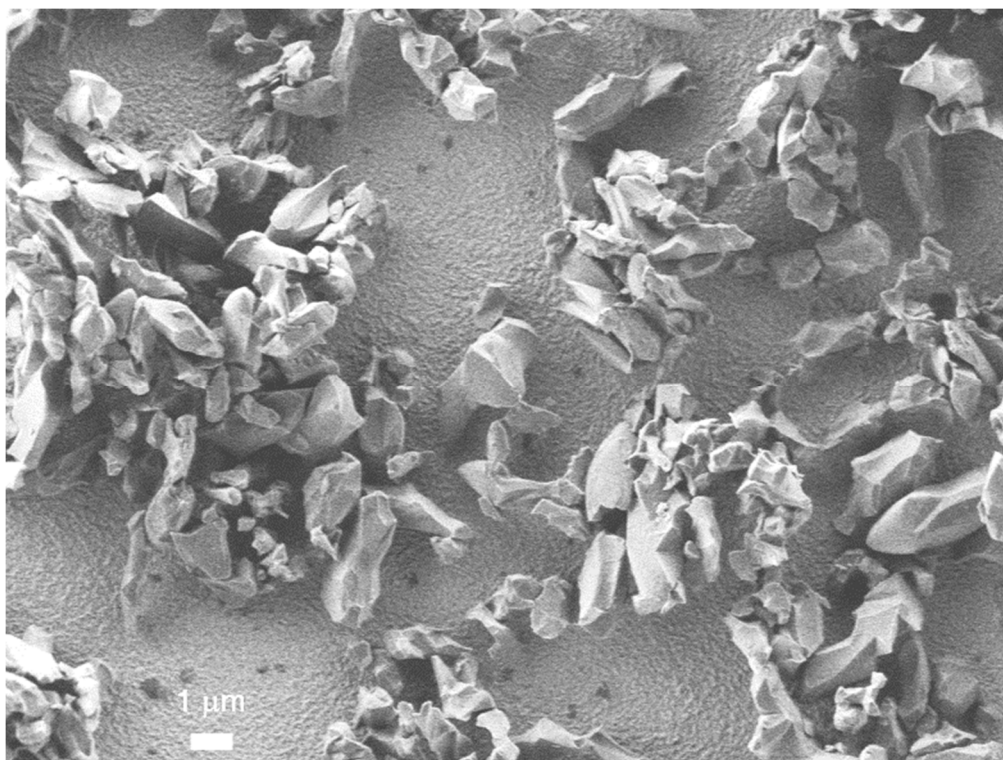


Figure S5. The SEM image of COF-300-T with the scale bar of 1 micrometer. The crystal sizes are distributed widely and the deformed shapes are generally observed.

1.4. Thermal Gravimetric Analyses

The thermal gravimetric analyses (TGA) were carried out using a TA Q50 TGA analyzer from 25 to 700 °C under N₂ atmosphere with temperature ramping rate of 5 °C/min.

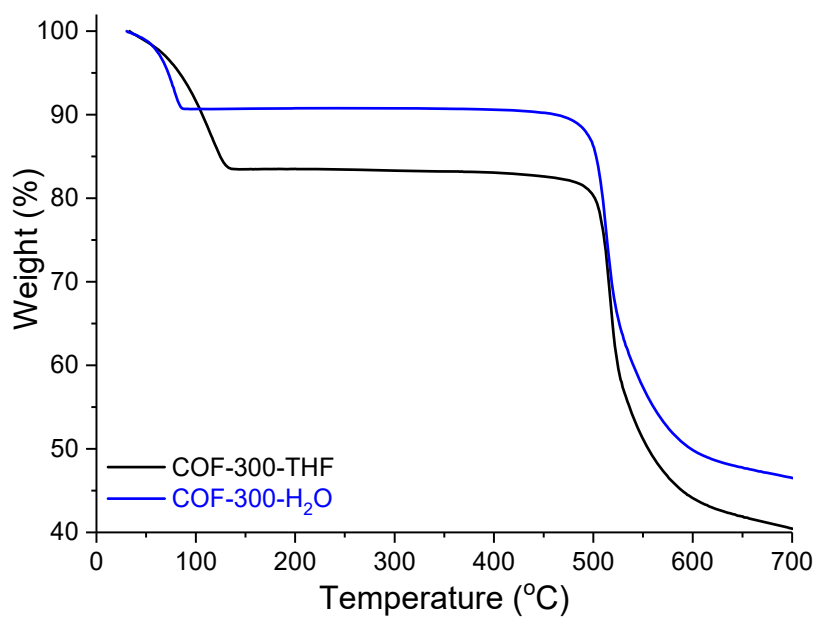


Figure S6. The TGA traces of COF-300-THF (black) and COF-300-H₂O (blue). High thermal stability is indicated up to 500 °C under N₂. The weight loss (~9.24%) before 100 °C for that of the COF-300-H₂O can be attributed to the water adsorbed in the pore, and the weight loss before 150 °C for that of the COF-300-THF can be attributed to the THF adsorbed in the pore.

1.5. Solid-State Nuclear Magnetic Resonance Spectroscopy

The solid-state ^{13}C nuclear magnetic resonance (NMR) spectra were recorded on a Agilent DD2 600MHz NMR spectrometer with cross-polarization magic angle-spinning (CP/MAS) and 3.2-mm double-resonance MAS probe. The samples were loaded in the zirconia rotor and with the sample spinning rate of 10.0 kHz.

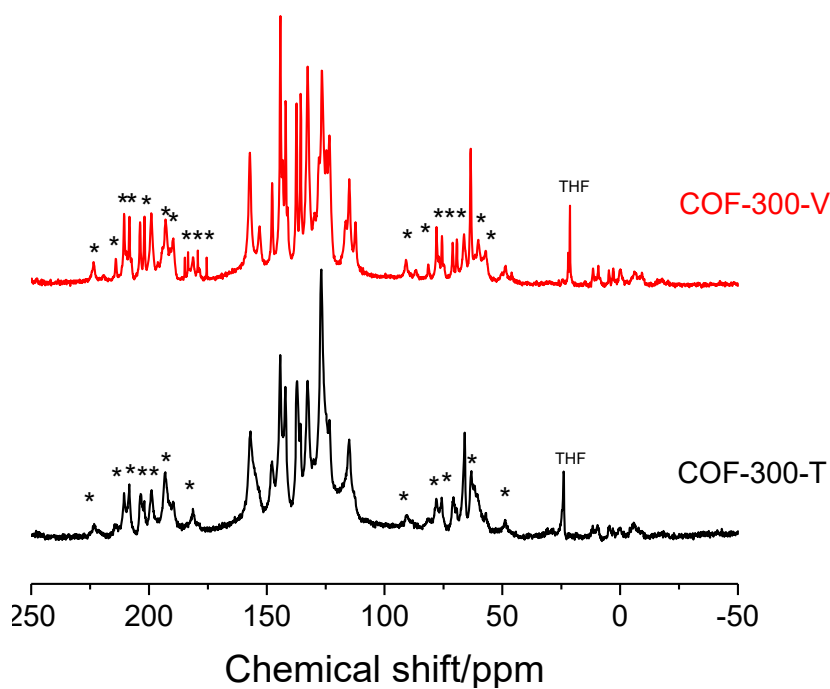


Figure S7. The ^{13}C solid-state NMR spectra of COF-300-V and COF-300-T. The pink broadness of COF-300-V is generally narrower than that of the COF-300-T.

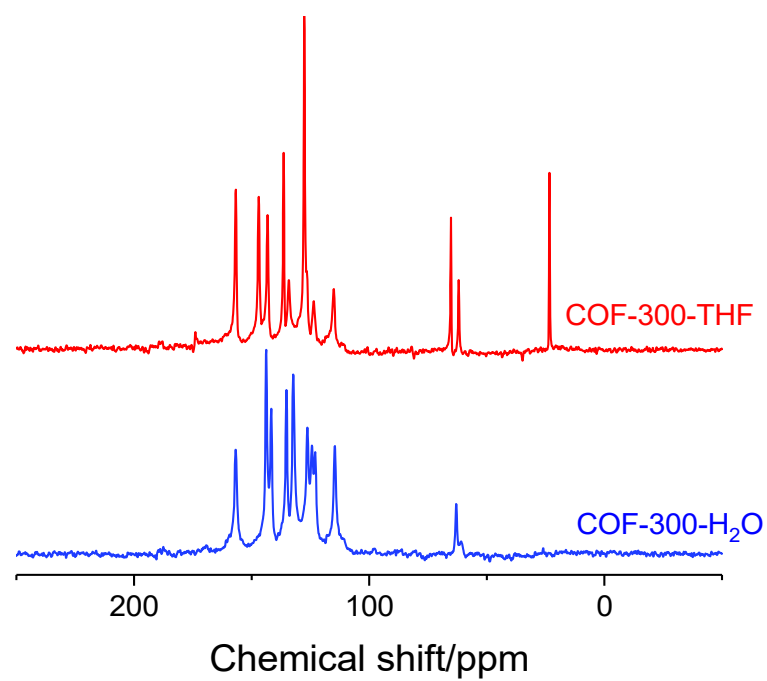


Figure S8. The ^{13}C solid-state NMR spectra of COF-300-THF and COF-300-H₂O. The structural transformation has caused the changes of chemical shifts.

Section S2. Structure Modeling and Rietveld Refinements

2.1. High-Resolution Powder X-Ray Diffraction Analyses

The high-resolution power X-ray diffraction (PXRD) patterns were collected at the beamline BL14B1 of the Shanghai Synchrotron Radiation Facility (SSRF)^[2] using X-ray with a wavelength of 0.6895 Å and transition model. The samples were held in glass capillary and kept spinning during the measurement. The guest-free COF-300-V was sealed in the glass capillary and heated at 100 °C under high vacuum overnight, and frame sealed in vacuum.

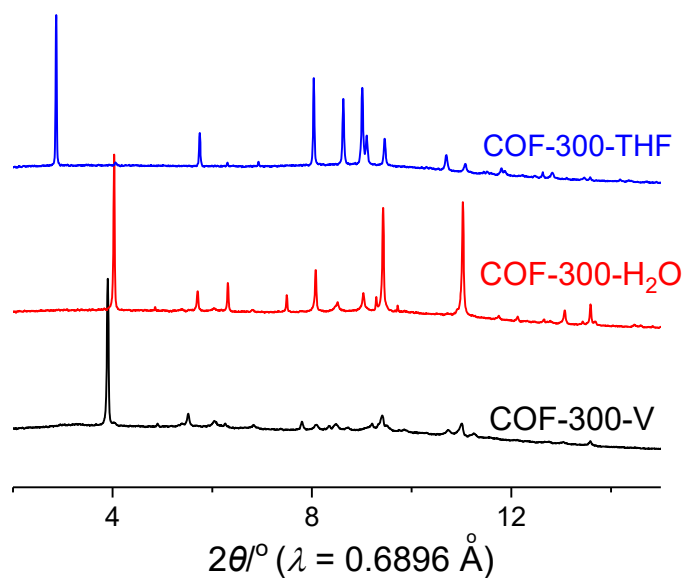


Figure S8. PXRD patterns of COF-300-THF (blue), COF-300-H₂O (red) and COF-300-V (black).

2.2. Structural modeling and Rietveld Refinement

The structure models were built by using the Crystal Building module using the space groups and unit-cell parameters obtained from the Pawley refinements, and then optimized by the Forcite module using the universal force field. Rietveld refinements were performed to the modeled structures, in which the peak profiles, zero-shift, background, and unit-cell parameters, Berar–Baldinozzi asymmetry correction parameters, preferred orientation and global isotropic temperature factors were optimized step by step to meet good agreement between the calculated and the experimental powder diffraction patterns.

Table S4. Rietveld refined cell parameters for COF-300-THF, COF-300-free and COF-300-H₂O.

COF-300	COF-300-THF	COF-300-V	COF-300-H ₂ O
Moiety Formula	C ₇₃ H ₉₂ N ₄ O ₈	C ₄₁ H ₂₈ N ₄	C ₄₁ H ₃₆ N ₄ O ₄
Formula Weight	1153.51	576.67	648.74
Crystal system	Tetragonal	Tetragonal	Tetragonal
Space group	<i>I4₁a</i> (No.88)	<i>I4₁a</i> (No.88)	<i>I4₁a</i> (No.88)
<i>Z</i>	4	4	4
Density(g/cm ³)	1.392	1.051	1.255
<i>a</i> (Å)	27.486(1) Å	20.353(3) Å	19.5861(8) Å
<i>b</i> (Å)	27.486(1) Å	20.353(3) Å	19.5861(8) Å
<i>c</i> (Å)	7.285(3) Å	8.796(2) Å	8.9482(6) Å
<i>V</i> (Å ³)	5503.7(5) Å ³	3644(1) Å ³	3432.7(4) Å ³
<i>R_p</i> (%)	4.76%	3.14%	4.87%
<i>R_{wp}</i> (%)	3.22%	2.24%	3.46%

Table S5. Crystal system, space group, unit cell parameters of COF-300-THF.

Space group: $I4_1a$ (No.88)							
$a = b = 27.486(1) \text{ \AA}$, $c = 7.285(3) \text{ \AA}$							
$\alpha = \beta = \gamma = 90^\circ$							
$V = 5503.7(5) \text{ \AA}^3$							
Atom	x	y	z	Atom	x	y	z
C1	0.38349	0.50656	0.90146	H24	0.41300	0.83516	1.13118
C2	0.42286	0.53779	0.91079	H25	0.39409	0.79119	0.97339
C3	0.45850	0.53685	0.77639	H26	0.37902	0.85179	0.73956
C4	0.45599	0.50397	0.62998	H27	0.43152	0.87546	0.85595
C5	0.41743	0.47081	0.62999	H28	0.33514	0.91751	0.8216
C6	0.38026	0.47286	0.75903	H29	0.37770	0.93967	0.97729
H7	0.42460	0.56357	1.02141	H30	0.29509	0.89530	1.10197
H8	0.48890	0.56156	0.78541	H31	0.35109	0.89863	1.22477
H9	0.41801	0.44129	0.53969	O32	0.19232	0.80071	0.88579
H10	0.35133	0.44627	0.75364	C33	0.23387	0.82514	0.94431
N11	0.34940	0.50897	1.04683	C34	0.23675	0.87184	0.83721
C12	0.30523	0.49311	1.04582	C35	0.20357	0.86420	0.67900
C13	0.27685	0.49752	1.21326	C36	0.18700	0.81216	0.70149
C14	0.27318	0.51009	1.54168	H37	0.23346	0.83119	1.09286
C15	0.29996	0.50788	1.38057	H38	0.26532	0.80145	0.92623
H16	0.29129	0.51939	1.66785	H39	0.27358	0.87743	0.78650
H17	0.33873	0.51452	1.38604	H40	0.22525	0.90274	0.92057
H18	0.71063	0.52406	0.92660	H41	0.22472	0.86853	0.55084
O19	0.33963	0.83483	1.08447	H42	0.17218	0.88956	0.68429
C20	0.38697	0.82875	1.01889	H43	0.20923	0.78690	0.61595
C21	0.39286	0.86585	0.87113	H44	0.14841	0.80727	0.66521
C22	0.35959	0.90644	0.93364	C45	0	0.5	0.25
C23	0.33387	0.88522	1.09642				

Table S6. Crystal system, space group, unit cell parameters of guest free COF-300-V.

Space group: $I4_1a$ (No.88) $a = b = 20.353(3)$ Å, $c = 8.796(2)$ Å $\alpha = \beta = \gamma = 90^\circ$ $V = 3644(1)$ Å ³							
Atom	x	y	z	Atom	x	y	z
C1	0.35571	0.51918	0.85808	N11	0.32052	0.52809	0.99678
C2	0.37455	0.57485	0.77654	C12	0.28753	0.48230	1.06516
C3	0.41732	0.56919	0.65336	C13	0.26520	0.49237	1.22107
C4	0.44151	0.50697	0.60866	C14	0.25450	0.56214	1.44312
C5	0.42135	0.45123	0.69127	C15	0.26913	0.55467	1.28946
C6	0.37904	0.45711	0.81416	H16	0.25731	0.93967	0.97729
H7	0.35839	0.62297	0.81364	H17	0.28449	0.59720	1.22421
H8	0.43456	0.61400	0.60023	H18	0.71934	0.56565	1.01397
H9	0.44210	0.40344	0.66643	C19	0	0.5	0.25
H10	0.36886	0.41360	0.88059				

Table S7. Crystal system, space group, unit cell parameters of COF-300-H₂O.

Space group: $I4_1a$ (No.88) $a = b = 19.5861(8)$ Å, $c = 8.9482(6)$ Å $\alpha = \beta = \gamma = 90^\circ$ $V = 3432.7(4)$ Å ³							
Atom	x	y	z	Atom	x	y	z
C1	0.35060	0.50015	0.85424	C12	0.30149	0.46144	1.08895
C2	0.35672	0.55728	0.76251	C13	0.27213	0.48091	1.23267
C3	0.40007	0.55637	0.63993	C14	0.23564	0.56854	1.40636
C4	0.43876	0.49773	0.60655	C15	0.25683	0.54947	1.26427
C5	0.43009	0.43953	0.69672	H16	0.22401	0.62161	1.42876
C6	0.38639	0.44033	0.81857	H17	0.26256	0.58846	1.18010
H7	0.33015	0.60393	0.79027	H18	0.68457	0.59119	1.07099
H8	0.40622	0.60323	0.57838	O293	0.25959	0.32006	0.76886
H9	0.46066	0.39461	0.67717	H294	0.29423	0.28362	0.75698
H10	0.38448	0.39535	0.88783	H295	0.26906	0.33768	0.87052
N11	0.31430	0.50826	0.99103	C19	0	0.5	0.25

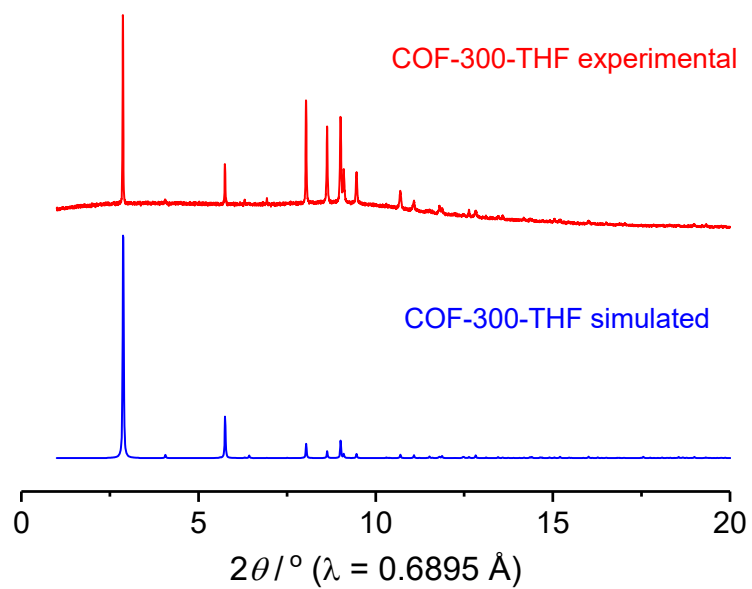


Figure S9. PXRD pattern COF-300-THF, compared to the simulated pattern.

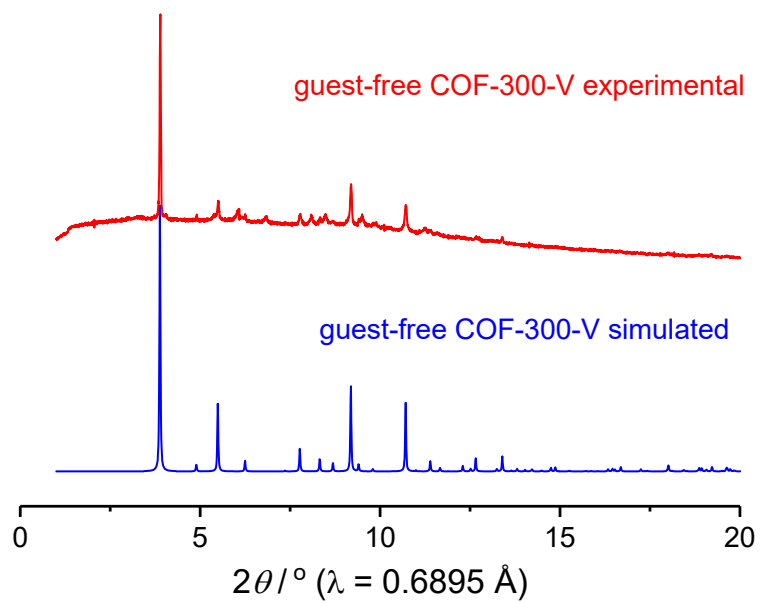


Figure S10. PXRD pattern guest-free COF-300-V, compared to the simulated pattern.

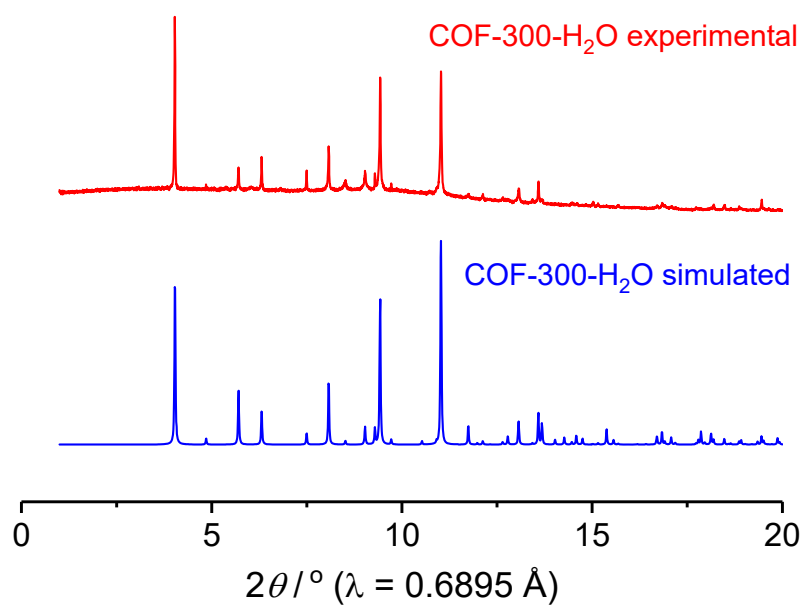


Figure S11. PXRD pattern COF-300-H₂O, compared to the simulated pattern.

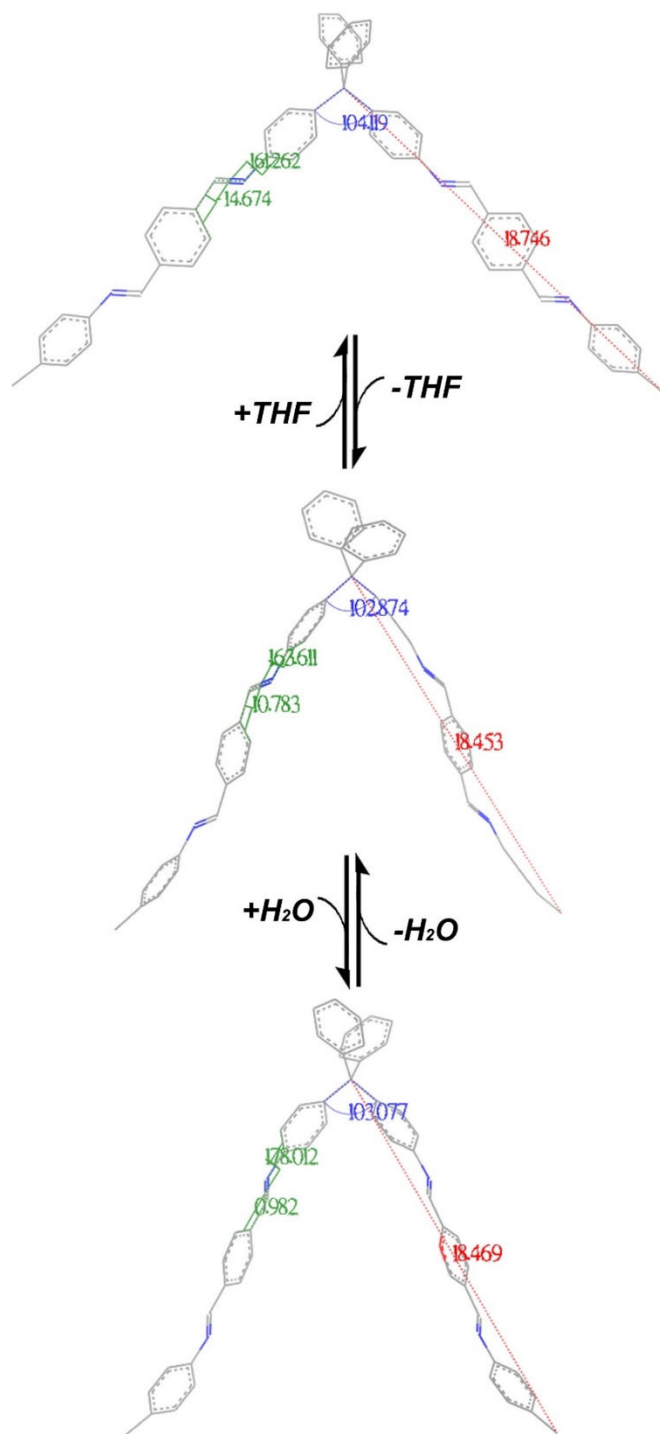


Figure S12. Conformation change of the organic linkers derived from the structure models of COF-300-THF, COF-300-free and COF-300-H₂O.

2.3 Reversibility of solvent effect of COF-300

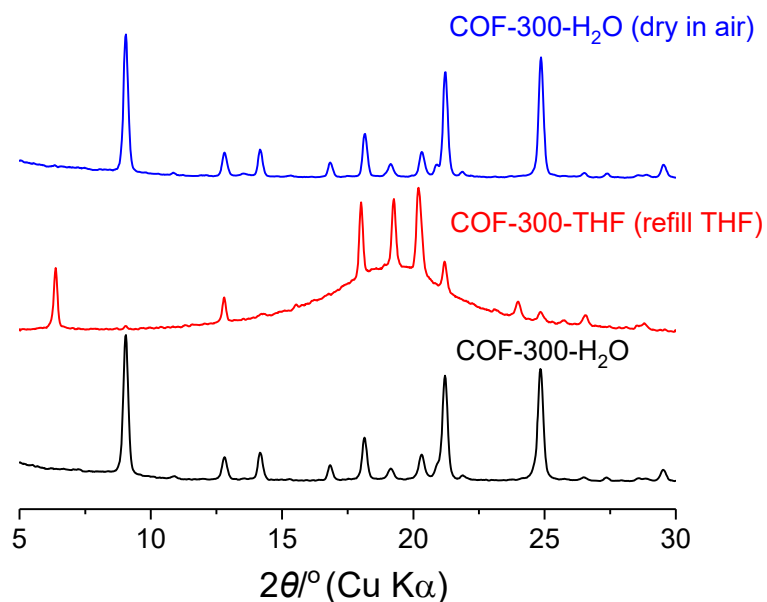


Figure S13. Experiment PXRD patterns COF-300-V in air (black) and fill with THF (red) and dry in air again (blue). The result shows the structural transformation of COF-300 could be repeated.

Section S3. Low Pressure Gas/Vapor Adsorption

Low-pressure gas adsorption isotherms were measured volumetrically using a Quantachrome iQ (N₂ and CH₄) or MicrotacBELsorp Max (CO₂) gas sorption analyzer. Liquid nitrogen bath was used for the temperatures controlled at 77K and 112K (with cryocooler); dry ice-methanol bath was used for the temperature controlled at 195K. Water bath with circulator were used for temperatures controlled at 273, 283 and 298 K. The organic vapor and H₂O adsorption isotherms were collected using MicrotracBELSopr-Aqua3 adsorption apparatus with a water circulator bath. Ultrahigh grade of gases such as He, N₂, CH₄ and CO₂, were used through all the experiments. Anhydrous solvents were used for vapor adsorption, which degassed at least five times before isotherm collection.

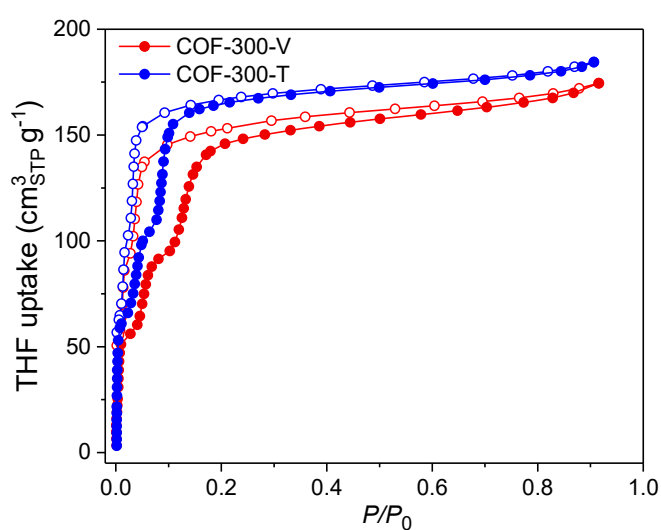


Figure S14. Comparison of THF vapor sorption isotherms of COF-300-V and COF-300-T at 283 K.

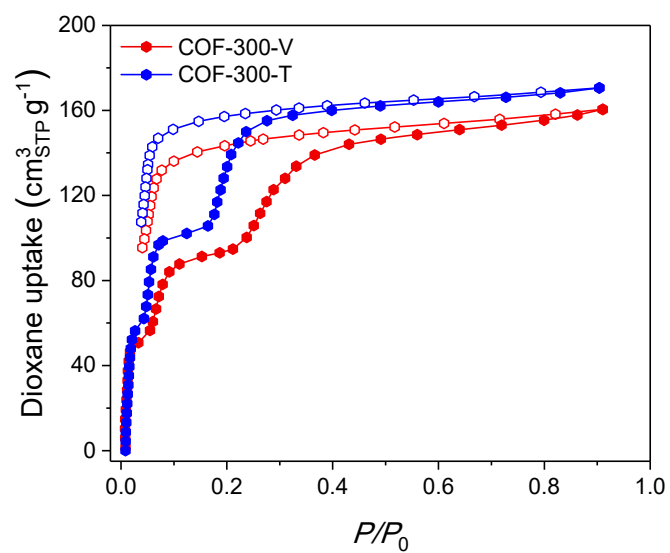


Figure S15. The 1,4-dioxane vapor adsorption isotherm of COF-300-V at 298 K.

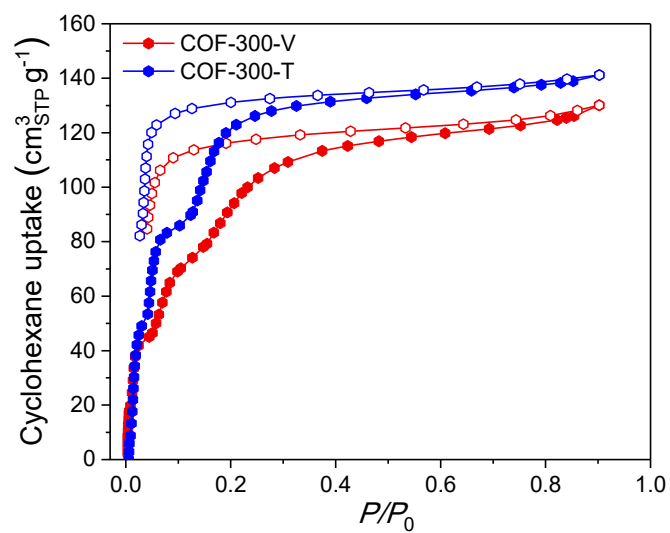


Figure S16. The cyclohexane vapor adsorption isotherm of COF-300-V at 298 K.

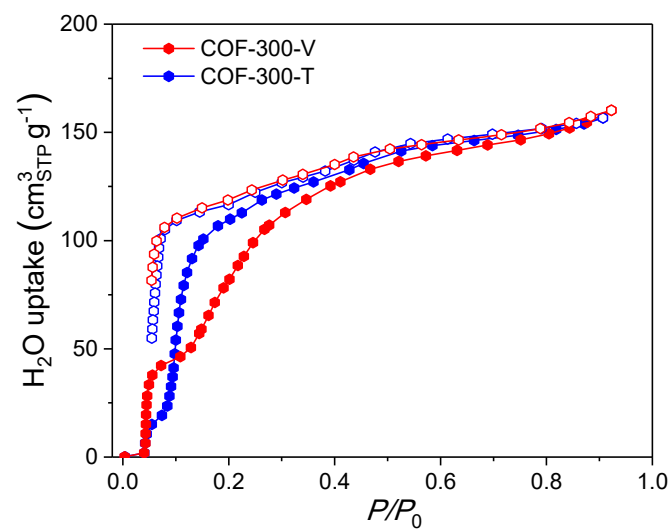


Figure S17. Comparison of the first-cycle water adsorption isotherms of COF-300-V and COF-300-T at 298K.

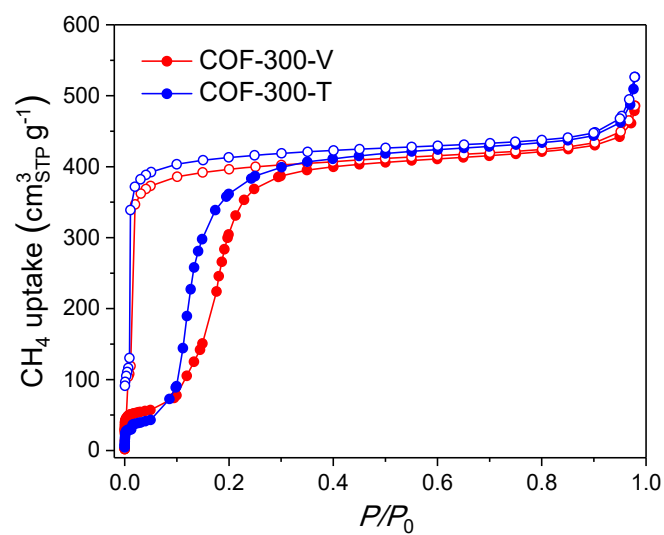


Figure S18. Comparison of the methane adsorption isotherms of COF-300-V and COF-300-T at 112 K.

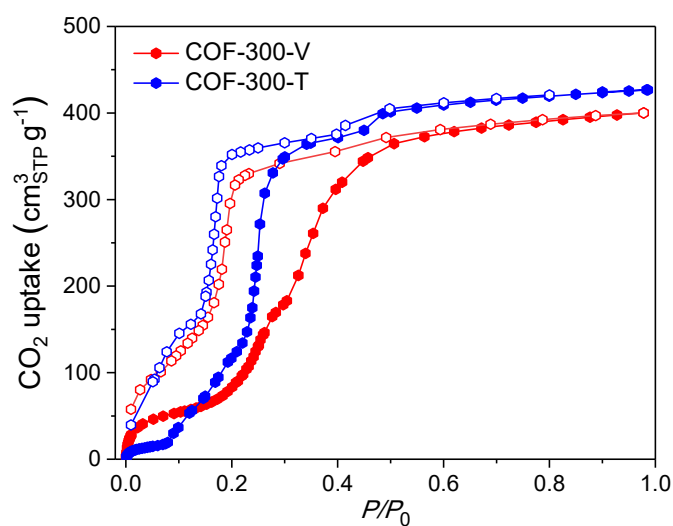


Figure S19. Comparison of the carbon dioxide gas adsorption isotherms of COF-300-T and COF-300-V at 195 K.

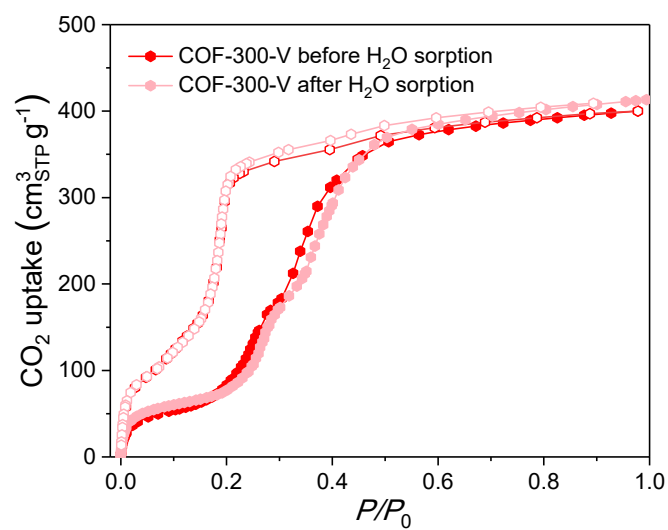


Figure S20. Comparison of the carbon dioxide gas adsorption isotherms of COF-300-V before and after water adsorption at 195 K.

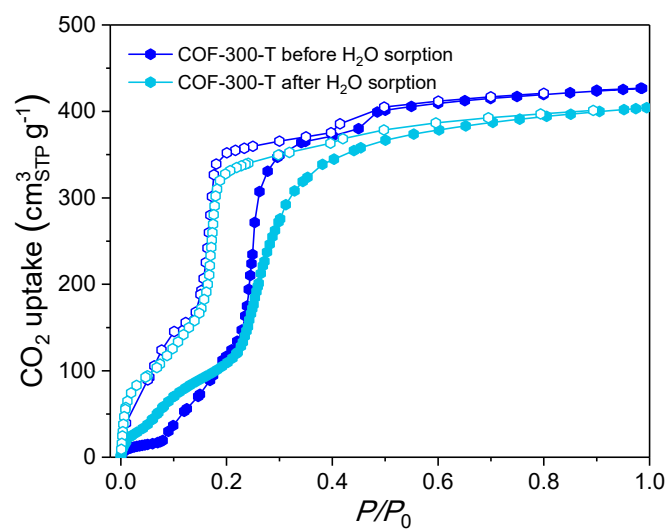


Figure S21. Comparison of the carbon dioxide gas adsorption isotherms of COF-300-T before and after water adsorption at 195 K.

Section S4. Gas Adsorption In-Situ PXRD Analyses

The gas adsorption in-situ PXRD patterns were collected on a Rigaku SmartLab diffractometer equipped with cryogenic holder and MicrotracBEL Max adsorption instruments. The sample were place in the chamber with Be windows, and the PXRD patterns were collected simultaneously with the adsorption isotherm. The sample was preheated and evacuated in the chamber before measurement.

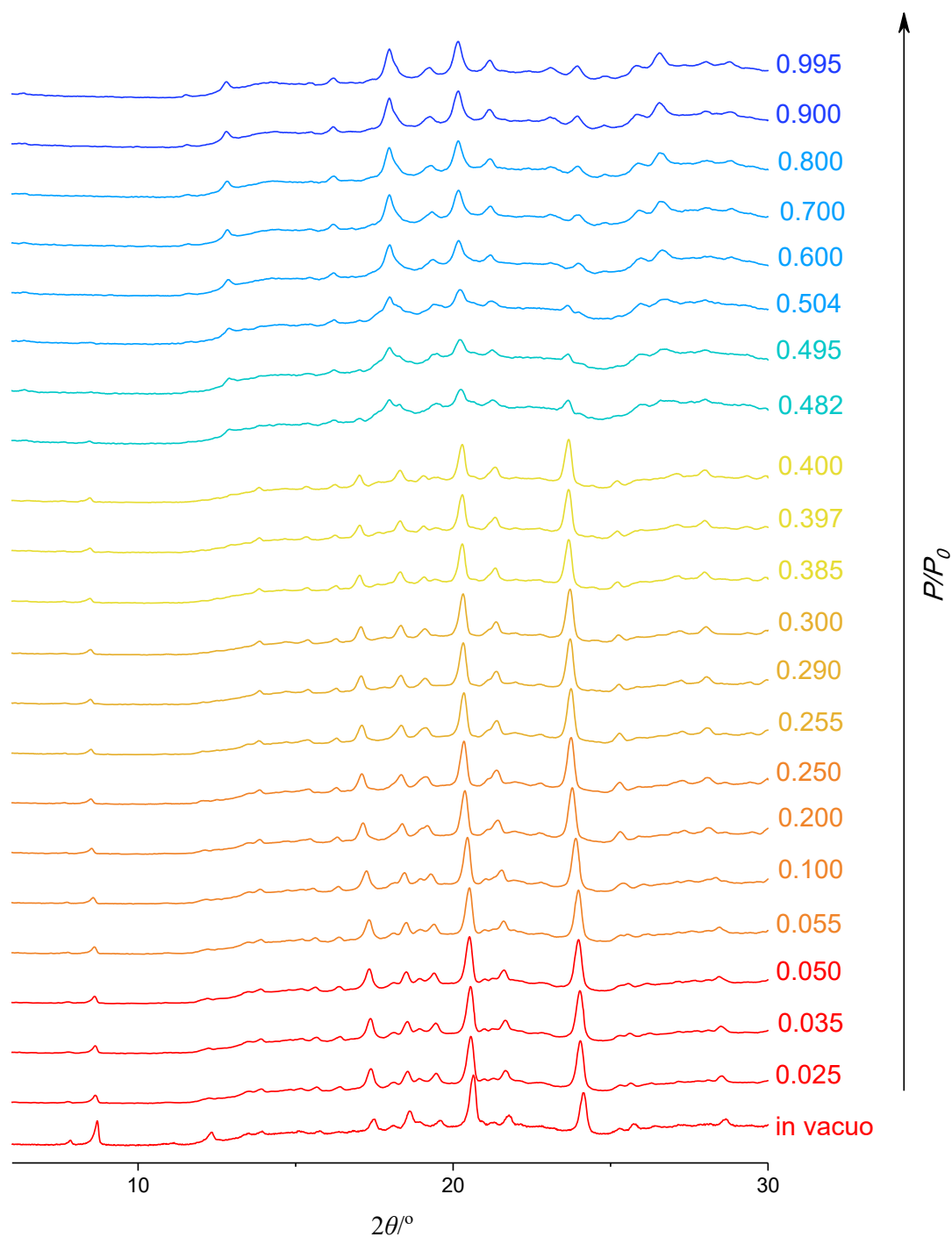


Figure S22. In-situ PXRD patterns of COF-300-V at different equilibrium pressures during adsorption of CO₂ at 195 K.

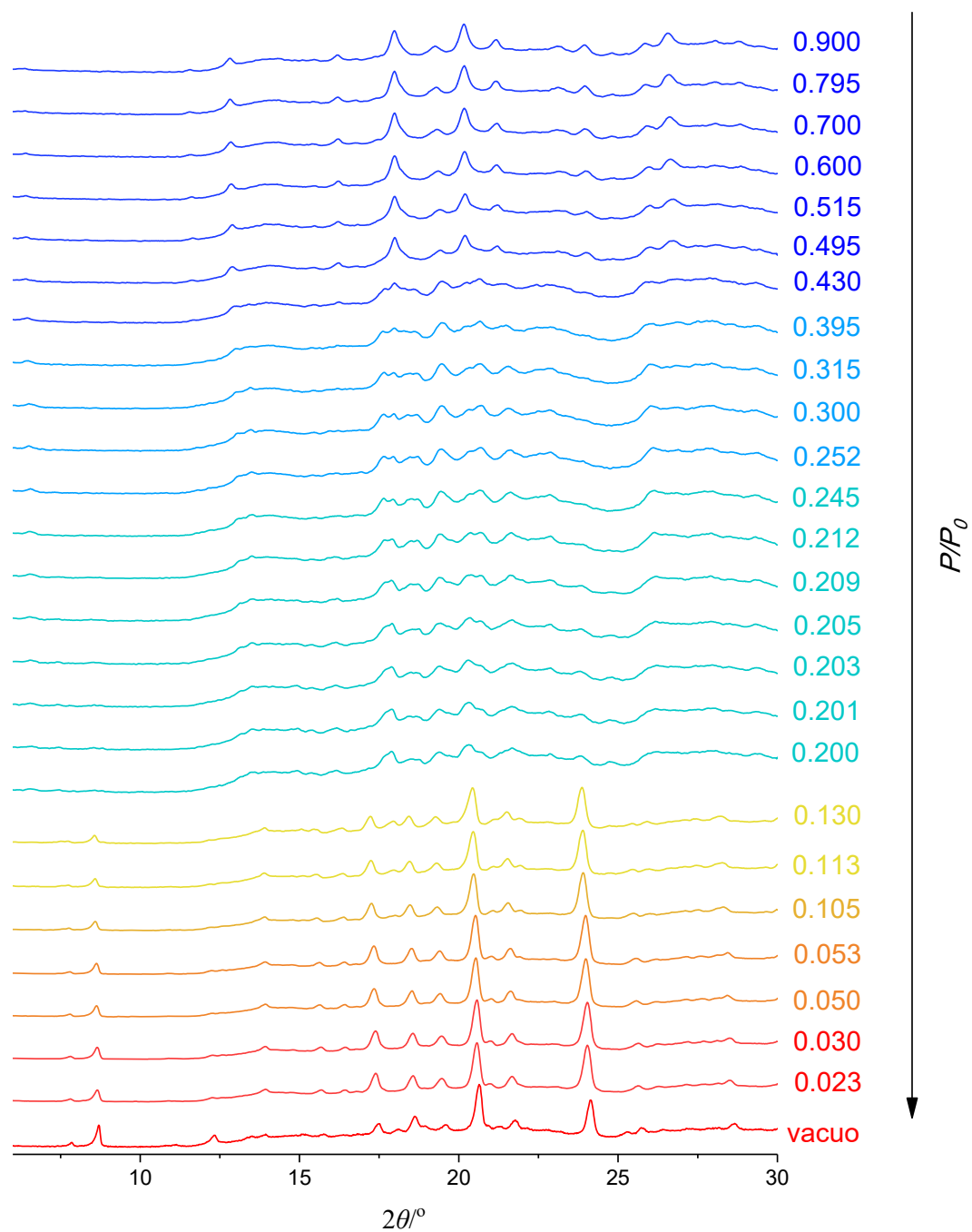


Figure S23. In-situ PXRD patterns of COF-300-V at different equilibrium pressures during desorption of CO₂ at 195 K.

References

- [1] (a) Plietzsch, O.; Schilling, C. I.; Toley, M.; Nieger, M.; Richert, C.; Muller, T.; Bräse, S. *Org. Biomol. Chem.* **2009**, *7*, 4734. (b) Ganesan, P.; Yang, X.N.; Loos, J.; Savenije, T.J.; Abellon, R.D.; Zuilhof, H.; Sudhölter, E.J.R. *J. Am. Chem. Soc.*, **2005**, *127*, 14530.
- [2] Yang, T.-Y.; Wen, W.; Yin, G.-Z.; Li, X.-L.; Gao, M.; Gu, Y.-L.; Li, L.; Liu, Y.; Lin, H.; Zhang, X.-M.; Zhao, B.; Liu, T.-K.; Yang, Y.-G.; Li, Z.; Zhou, X.-T.; Gao, X.-Y. *Nuclear Sci. Tech.* **2015**, *26*, 020101.